Effect of Surface Mechanical Attrition Treatment (SMAT) on the Surface and Electrochemical Characteristics of Pb-Sn Alloy

T. Balusamy[1,2], M. Venkateswarlu[2,], K.S.N. Murthy[2], S. Vijayanand[2] and T.S.N. Sankara Narayanan[1,3,*]*

[1]CSIR-National Metallurgical Laboratory, Madras Centre, CSIR Complex, Taramani, Chennai-600 113, India
[2]R & D, Amara Raja Batteries Limited., Karakambadi -517520, Andhra Pradesh, India
[3]Department of Dental Biomaterials, School of Dentistry, Chonbuk National University, Jeonju, South Korea
[*]E-mail:mvu@amararaja.co.in (M.Venkateswarlu);tsnsn@rediffmail.com (T.S.N. Sankara Narayanan);

The influence of surface mechanical attrition treatment (SMAT) on the mechanical and electrochemical properties of Pb-Sn alloys is presented. SMAT induced plastic deformation of the Pb-Sn alloy to a depth of $\sim$ 43 μm from the top surface and enabled the formation of a graded layer structure. In spite the increase in average surface roughness (R_a) from 0.40 to 2.42 µm, the uniform dimple-like features generated on the surface of the Pb-Sn alloy helped to improve the interfacial characteristics of active material and grid. SMAT has also enabled a marginal increase in hardness of the Pb-Sn alloy. The electrochemical behavior of the Pb-Sn and treated alloy was evaluated by employing potentiodynamic polarization, electrochemical impedance spectroscopy (EIS) and cyclic voltammetry (CV) techniques. The ability of the treated surface to induce passivation offered an increase in corrosion resistance. The current density of the redox reaction profile suggests good charge-discharge characteristics of the SMATed Pb-Sn alloy.

1. INTRODUCTION

Lead acid batteries are the most promising and reliable energy storage systems that are widely used in automotive and industrial applications [1, 2]. The life of these batteries depends on the electrochemical and mechanical properties of the grid made out of lead and lead alloy. The function of the grid is to act as a current collector and also supportive to the active material. It has been reported

that the positive grid is more prone to corrosion than the negative grid in the acid environment [3-5]. Therefore, the thickness of the positive grid is designed thicker than the negative grid in order to prolong the cycle life of the battery. The increase of grid weight would add up overall weight of the battery in turn decrease in the energy density. The pure lead is soft in nature and is alloyed with different metals such as calcium, antimony, tin, tellurium, strontium, etc., to improve its fluid characteristics and mechanical properties as well [3-14]. The lead alloy grids are commonly produced by gravity casting and resultant grid properties depend on alloy composition and process conditions as well. These two attributes have a remarkable influence on the surface morphology, micro-structure and solute re-distribution of the end product [15-19]. It is imperative that the battery grids should possess sufficient mechanical strength and corrosion resistance to withstand repeated cycling operations. Plastic deformation processes such as rolling, extrusion, etc., have been explored and the utility of such methods to improve the properties of the lead alloys have been reported elsewhere [20-22]. The rolled and expanded grids (plastically deformed) exhibit uniform surface attack without any significant change in the granular structure as compared to the cast-strip, expanded grids [23]. Surface modification methods such as physical vapour deposition (PVD), chemical vapour deposition (CVD), shot peening, surface mechanical attrition treatment (SMAT), etc., have been shown to improve the physical, mechanical and electrochemical properties of materials [24-27].

SMAT is a novel surface treatment method, which enables surface nanostructuring of metallic materials [28, 29]. In this method, the surface modification is effected through grain refinement mechanism induced by plastic deformation. SMAT induces compressive residual stress and increase the hardness [28, 29]. Its ability to provide a uniform surface profile and impart passivation of the surface would help to increase the interfacial characteristics and corrosion resistance. In this perspective, the present study aims to explore the possibility of using SMAT to impart the desirable characteristics to the Pb-Sn alloy and also to evaluate its surface characteristics, electrical and electrochemical behavior in aqueous sulphuric acid so as to ascertain its suitability as a grid material for lead acid batteries.

2. EXPERIMENTAL DETAILS

The Pb-Sn alloy was prepared by melting of pure lead and tin mixture at 525 ± 20 °C. The resultant molten liquid was poured into a mould by direct casting process and then allowed to solidify. The tin content in the lead alloy is ~1.20-1.27 wt. %. The Pb-Sn alloy having dimension of 70 mm x 70 mm and 3 mm thickness samples were used for surface modification by SMAT (Surface nano-crystallization equipment, Model: SNC1, SNC Adv. Tech. Co., Ltd., Chengdu, China). The schematic and process details of the SMAT have been described elsewhere by Lu and Lu [28, 30]. The Pb-Sn alloy was fixed at the upper part of the sample pot. The stainless steel (AISI 316L) balls with 2 mm ∅ (hereafter referred as SS balls) was, placed at the bottom of the pot, used to peen the surface of the Pb-Sn alloy during SMAT. The distance between the alloy sample and the SS balls was 28 mm. The sample pot was evacuated by rotary pump before treatment and maintained the pot pressure (-1bar) during treatment. The sample pot was connected to the vibration generator and the frequency of

vibration is kept constant at 50 Hz. The time duration of the SMAT process was limited to 15 min by considering the nature of the Pb-Sn alloy.

The untreated Pb-Sn (ULA) and treated Pb-Sn (TLA) alloys (hereafter referred as ULA & TLA) were characterized to understand the surface profile & topography, hardness, electrical and electrochemical behavior of alloy samples by employing respective techniques. The microstructural characteristics and extent of plastic deformation was determined by Optical microscopy (Union, Versamet 3). The structural characteristics and phase changes in the samples was determined by X-ray diffraction (XRD) (GE Inspection Tech, XRD 3003 TT, Germany) technique. The XRD pattern was recorded using Cu-K$_\alpha$ radiation (λ =1.5406 Å) in the range of 2θ from 20 to 90° at a scan rate of 0.02 per second. The surface profile of both ULA and TLA samples was measured using a surface profilometer (Mitutoyo SJ 301) while their surface topography was assessed using a Stereo microscope (Seiwa Japan & eM power image analyzer, India). The hardness of the ULA and TLA samples were measured using Vickers hardness tester (VM 50, Blue star FIE, India). The electrochemical characteristics of the ULA and TLA samples were evaluated using an electrochemical battery cycling tester (WonATech & VMPG 1000) coupled with IVMAN software for analysis. The Pb-Sn alloy samples were prepared by abraded sequentially using a series of SiC coated abrasive papers (120, 220, 400, 600, 800 and 1000 grit size), washed with deionized water followed by ethanol, and dried out using a stream of compressed air. The electrochemical studies were carried out using a three electrode cell that consists of the working electrode (ULA / TLA), counter electrode (platinum foil), and a reference electrode (Hg/Hg$_2$SO$_4$). The aqueous H$_2$SO$_4$ (specific gravity of 1.245) was used as electrolyte for electrochemical measurements carried out at 27 ± 1 ºC. All the three electrodes were arranged in a conventional flat electrochemical cell in such a way that the working electrode with an electrode area of 1cm^2 was exposed to electrolyte solution. The potentiodynamic polarization studies were carried out in the potential range of ± 200 mV at a scan rate of 1 mV/s. The corrosion potential (E$_{corr}$) and corrosion current density (i$_{corr}$) were calculated using Tafel extrapolation method. The electrochemical impedance spectroscopy (EIS) studies also have been carried out using electrochemical Impedance Analyzer (Zener BAS, IM6, Germany) on the ULA and TLA samples at their open circuit potentials (OCVs) in the frequency range from 0.1Hz to 10 KHz at excitation voltage of 5 mV. Cyclic voltammograms (CVs) of ULA and TLA samples were recorded in the potential range from 0.5 V to 1.7 V at a scan rate of 10mV/s. All the electrochemical measurements were performed at ambient conditions subject to pre-polarization of the sample at -1.65 V versus Hg/Hg$_2$SO$_4$ to remove the formation of oxide layer on the surface of Pb-Sn alloy.

3. RESULTS AND DISCUSSION

3.1. Structural characteristics

The cross sectional view of the optical micrographs of the TLA is shown in the Fig. 1. The micro-structural features indicate that the Pb-Sn alloys have undergone plastic deformation during SMAT process and the depth of deformation is ~ 43 μm. In addition, the deformation also leads to the formation of a graded layer structure, which would helps to improve mechanical property of the

sample. The formation of graded layer structure is due to the difference in strain and strain rate from top surface to the bulk. The formation of a graded layer structure has also been observed for other materials treated by SMAT [29, 30].
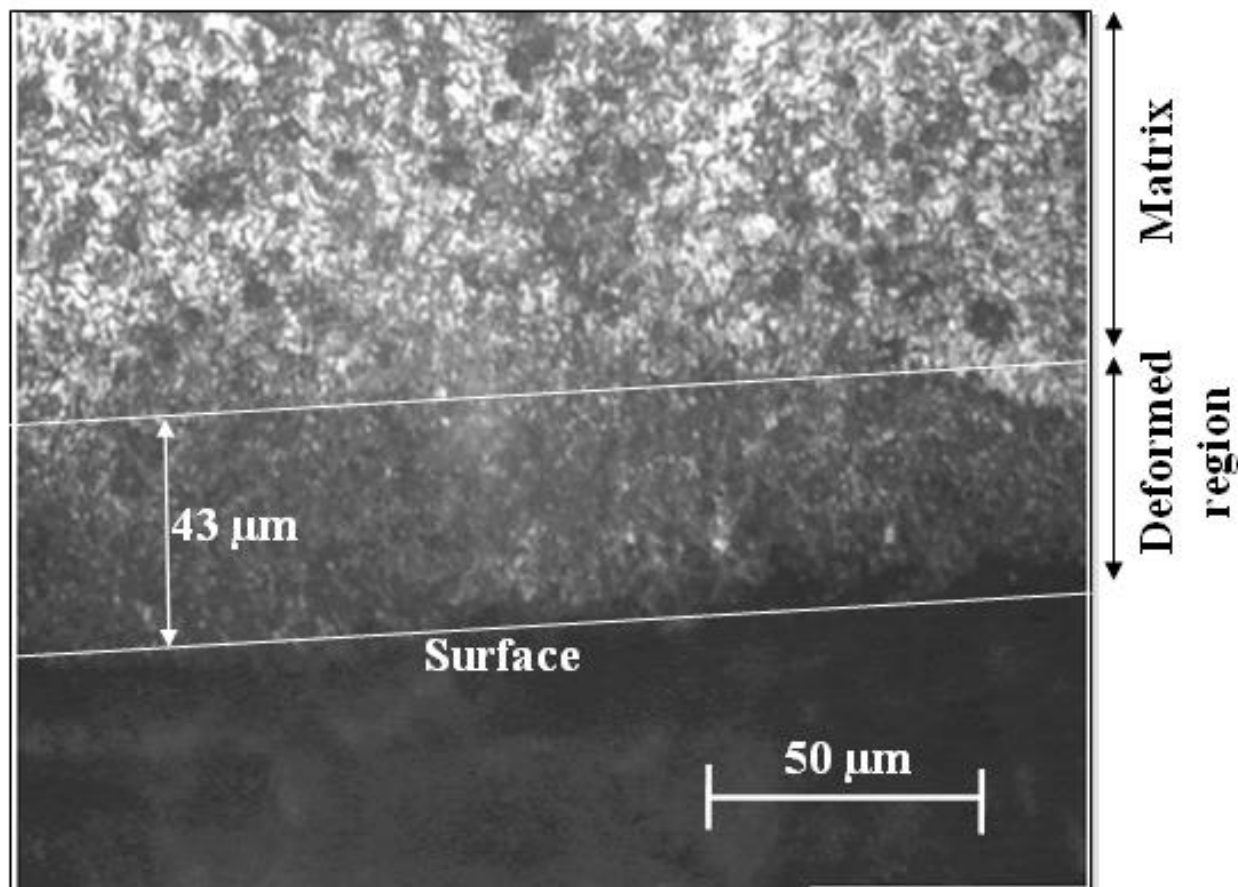

Figure 1. Cross sectional view of the optical micrographs infer deformed region of the TLA.

The recorded X-ray diffraction patterns of the ULA and TLA samples are shown in the Fig. 2 (a) and are indexed by comparing with the standard JCPDS pattern of lead (card no: 04-0686). The observed both the XRD pattern is exhibits good matching with standard JCPDS pattern of lead. The grain size for the ULA and TLA, estimated by Scherer's formula, is 51 nm and 54 nm, respectively.

The observed small peak in the XRD pattern at a diffraction angle of 28.9° could be assigned to PbO (101) that could be formed by aerial oxidation of the Pb-Sn surface after SMAT. It is observed that the characteristic peak intensity of Pb (111) plane of the TLA increased as compared to ULA and also slightly shifted towards the lower diffraction angle, as shown with dotted lines in Fig. 2(b). The increase in the peak intensity could be due to dynamic recrystallization of the TLA by considering the physical (softness, melting point, etc.) properties of the lead alloys.
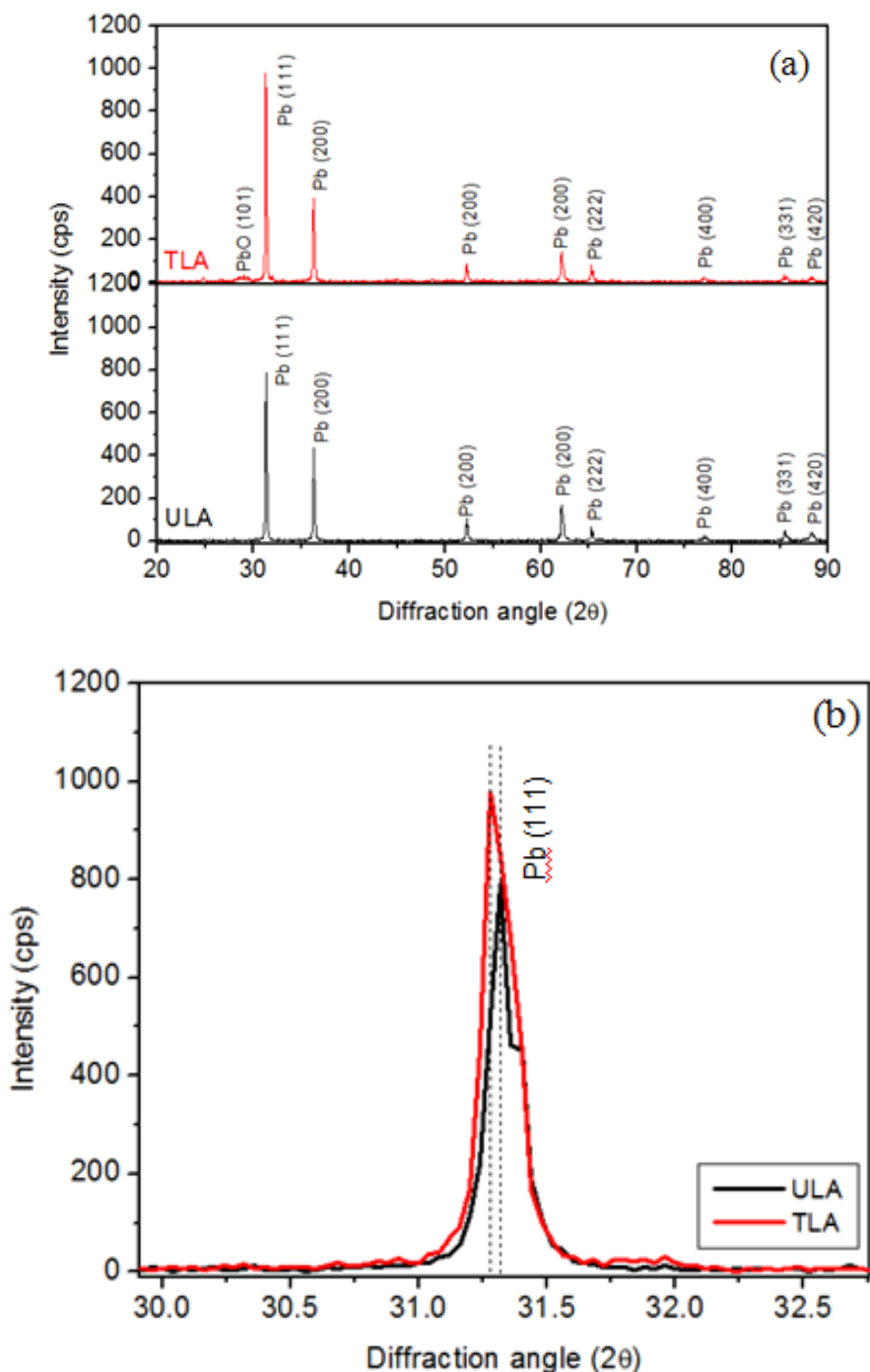
Figure 2. XRD patterns of the ULA and TLA (a); and expanded view of 2Θ scale from 30 to 32.5 degrees of the Pb (111) plane (b).

The Pb-Sn alloy is plastically deformed by the impingement of the surface with SS balls and might have accommodated the lattice strain induced by SMAT process. The similarity in grain size and marginal increase in hardness also suggest such possibility. The change in the lattice parameter (ULA: 4.9420 Å; TLA: 4.9480 Å), lattice strain (TLA: 0.0012) and the unit cell volume (ULA: 120.70026 Å^3; TLA: 121.1404 Å^3) confirms this attribute.

3.2. Surface profile and topography

The surface profiles and images of the surface topography of the ULA and TLA are shown in Figs. 3 (a & b and c & d), respectively. Obviously, the surface roughness of the TLA is much higher due to impingement of the SS balls on the surface of the sample. The average surface roughness (R_a) of the TLA increases to 2.42μm (Fig. 3(b)) which is significant as compared to the ULA (0.4μm) (Fig. 3(a)). Comparing the surface topography of the ULA and TLA (Figs 3 (c) & (d)); the TLA is generated very small dents in the form of dimples due to impingement of the SS balls on the surface of the Pb-Sn alloy. The surface roughness and dimple size and its distribution in the samples are the function of type and size of balls, frequency of vibration, mechanical properties of the alloy and treatment time [31-33]. Singh Mann et al [34] have been reported that the increase of surface area by small indentations on the lead alloy strip provide desired surface topography to improve the bonding between grid and active material interface. A rough surface could prevent the formation of plate like $PbSO_4$ crystals that are consider to be responsible for rapid capacity loss [1].
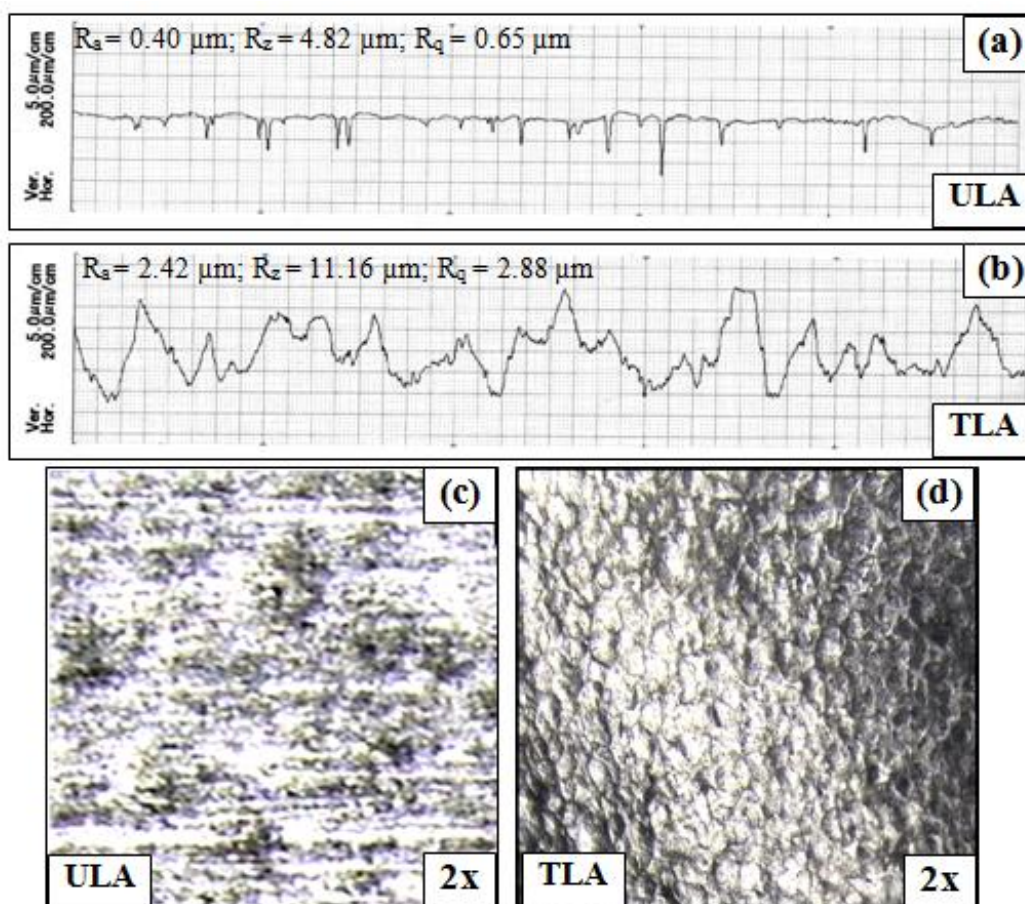

Figure 3. Surface profiles (a) & (b); and surface topography (c) & (d); of the ULA and TLA.

The generation of uniform surface profile and surface roughness with dimple-like features of the TLA is to improve the interfacial characteristics of the grid and active material which in turn eliminate the shedding.

3.3. Hardness

The dimensional stability of the lead/lead alloy grid is important parameter to be considered while designing the battery. A good mechanical strength and better corrosion resistance of the lead alloy could offer a service life of the battery. The SMAT enables a marginal increase (~ 4%) in hardness from17.5 ± 1 to 18.4 ± 0.8 VH_{1kgf} due to plastic deformation following the impingement of the SS balls. The similarity in the grain size and hardness of the alloys samples before and after the SMAT process and accommodation of the lattice strain further support the hardness values of the sample.

3.4. Potentiodynamic polarization studies

The corrosion behavior of lead alloys is of particular interest in terms of increase of life of the lead-acid batteries. The polarization curves of the ULA and TLA obtained in H_2SO_4 (specific gravity of 1.245) at 27 ± 1 ℃ is shown in the Fig. 4.
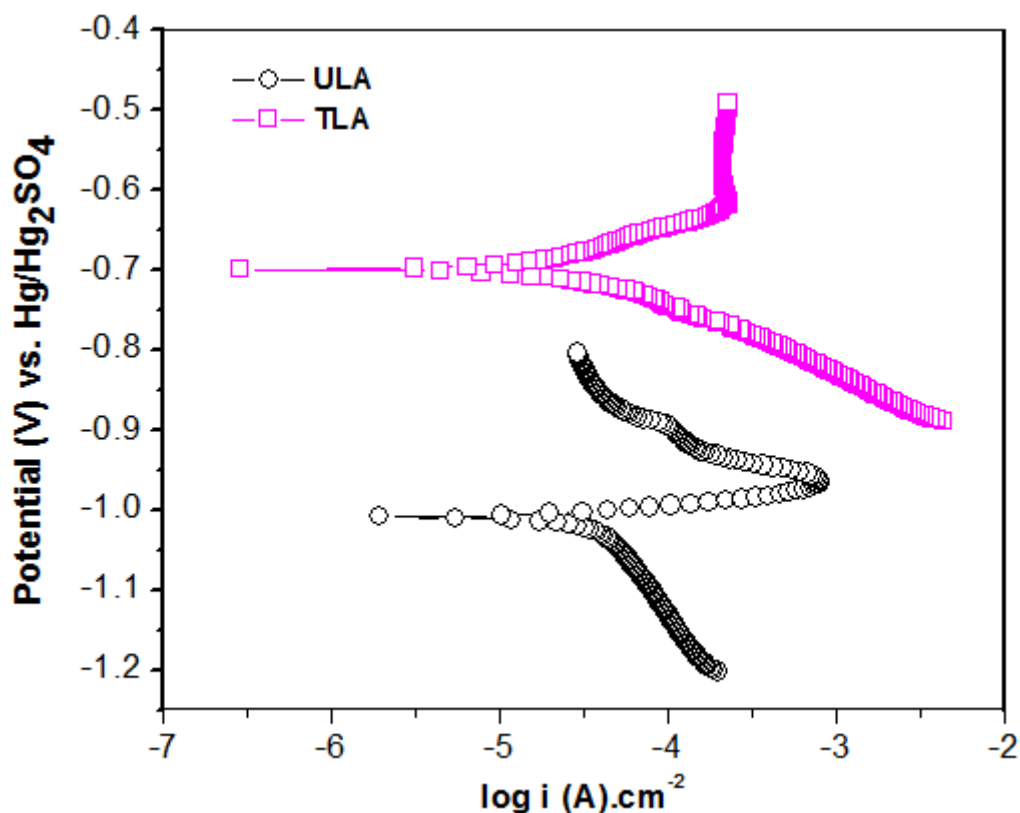

Figure 4. Potentiodynamic polarization curves of the ULA and TLA in H_2SO_4 (specific gravity: 1.245) at their OCPs.

It is evident from the Fig. 4 that there is a significant change in the cathodic and anodic reaction kinetics of the TLA. The E_{corr} values of the ULA and TLA are -1.009 V and -0.699V versus Hg/Hg_2SO_4 electrode and corresponding i_{corr} values are 27.86 and 17.10 $\mu A/cm^2$, respectively. The

anodic shift ($\sim$ 310 mV) in the E_{corr} of the TLA could be due to formation of an oxide film on the surface of the Pb-Sn alloy during aerial oxidation after SMAT. The development of PbO on the surface, as confirm in the XRD pattern, is believed to be responsible for the considerable anodic shift in potential of the TLA. A similar trend in the anodic shift (E_{corr}) was observed for AZ91D Mg alloy after SMAT using SS balls for 30 min [35]. In case of the ULA, the partial stabilization of the current density at the potential of -0.87 V indicates the precipitation and dissolution mechanism of $PbSO_4$ particles. On the other hand this phenomenon is not observed for the TLA. The passive current density of the TLA is higher when compared to the ULA is attributed to the formation of oxide film on the sample.

3.5. Electrochemical impedance spectroscopy studies

The Nyquist plots of the ULA and TLA in H_2SO_4 (specific gravity of 1.245) at 27 $\pm$ 1 °C are shown in the Fig. 5 (a). From the Fig. 5, it was observed that the ULA exhibits a semicircle followed by a long tail, respectively, in the higher (10^4 - 10 Hz) and lower frequency (10 – 0.1 Hz) regions. The inset in the Fig. 5 (a) shows the expanded view of lower frequency region of the ULA. On the other hand, the TLA also exhibits a semi-circle in the frequency region (10^4 - 1.0 Hz) of the spectra.

The EIS spectra of the ULA and TLA are characterized by a capacitive loop in higher frequency region and a tail in lower frequency region, suggests the involvement of two time constants. An equivalent electrical circuit model (EECM) is used to explain the EIS spectra of the ULA and TLA and the physical model is shown in the Fig. 5 (b). In this model, R_s represents the solution resistance, R_f is the film resistance, which is in parallel to the double layer capacitance, CPE_1. Further, a constant phase element, CPE_2 and charge transfer resistances, R_{ct}, are also included in the physical model to account for metal/film interface resistance. Peixoto et al. [19] have used a similar model to explain the electrochemical behavior of Pb-Sn alloy in 0.5 M H_2SO_4 solution.

The validity of this model is confirmed based on the non-linear least square fitting of the experimental data within the 5% error and the fitting results are given in Table. 1. The Bode impedance and Bode phase angle plots of the ULA and TLA are shown in Fig. 6. The |Z| at 0.1 Hz for the ULA and TLA is 106.26 ohm.cm^2 and 471.47 ohm.cm^2, respectively. The phase angle maximum (θ_{max}) for the ULA and TLA is 58.3° (@582 Hz) and 69.9° (@31.4 Hz), respectively. The higher |Z| and phase angle further substantiate the better corrosion behavior of the TLA when compared to the ULA [19].
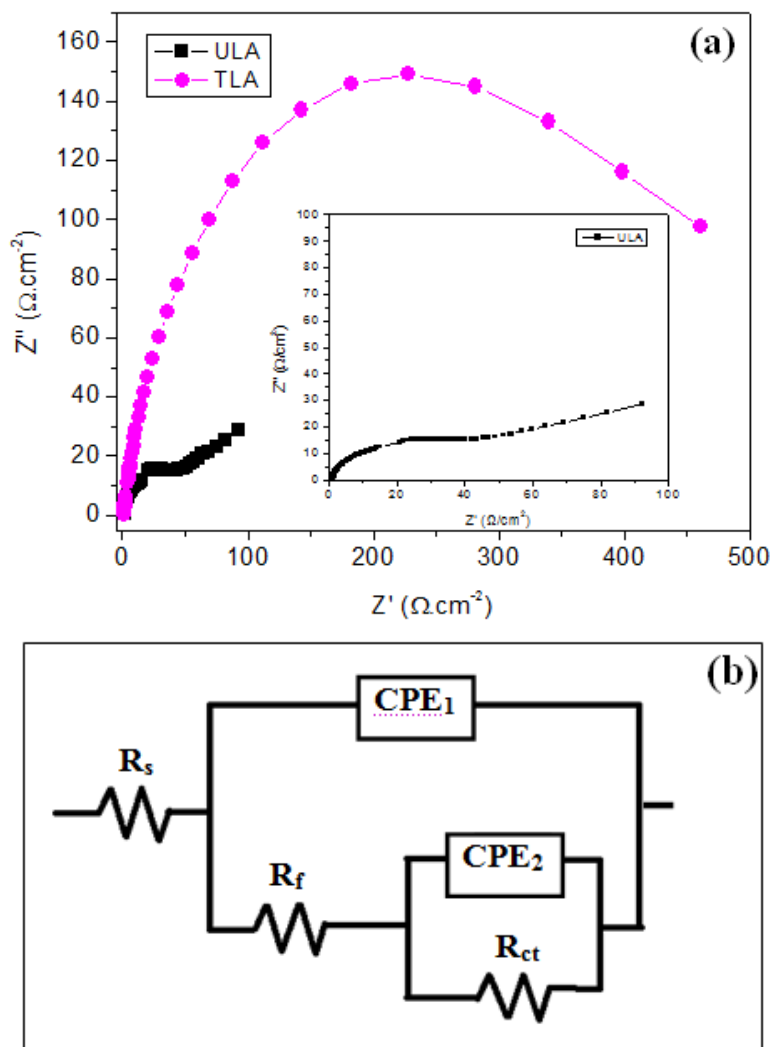
Figure 5. The Nyquist plots of the ULA and TLA obtained in H_2SO_4 (specific gravity: 1.245) at their OCPs. (a); and Equivalent circuit model (b).

Table 1. EIS parameters obtained from the Nquist plots of the ULA and TLA.

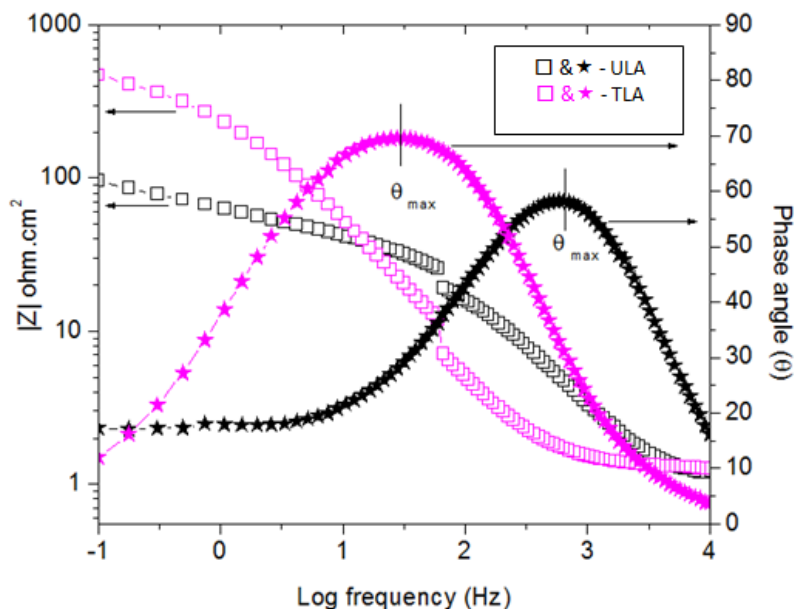| EIS parameters	ULA	TLA
R_s (Ohm.cm^2)	1.08	1.36
CPE_1 (S.s^n.cm^{-2})	1.53×10^{-4}	7.64×10^{-4}
CPE_2 (S.s^n.cm^{-2})	1.03×10^{-2}	2.31×10^{-4}
n_1	0.87	1
n_2	0.56	0.65
R_f (Ohm.cm^2)	36.32	407
R_{ct} (Ohm.cm^2)	108.9	68.55
χ^2	59×10^{-4}	36×10^{-4}

Figure 6. Bode impedance and bode phase angle plots of the ULA and TLA in H_2SO_4 (specific gravity:1.245).

3.6. Cyclic voltammetric studies

The Cyclic Voltammetric (CV) profiles for the ULA and TLA were recorded for 100 cycles in H_2SO_4 (specific gravity of 1.245) at 27 ± 1 ºC. The CV profiles of 1st, 25th, 50th, 75th and 100th cycles of the ULA and TLA respectively are shown in the Fig. 7(a & b).
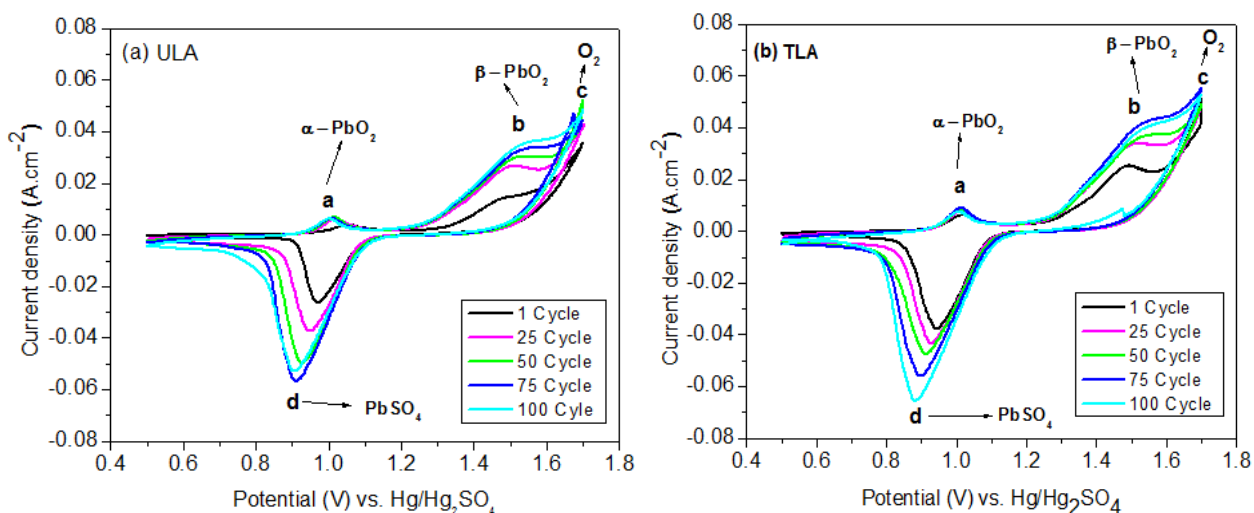

Figure 7. Cyclic voltammograms recorded for 100 cycles of the ULA (a); and TLA (b); in H_2SO_4 (specific gravity: 1.245).

The observed anodic peaks in the potential range of 1.00-1.05 V (marked as 'a') and 1.47-1.55 V (marked as 'b') versus Hg/Hg_2SO_4 electrode are corresponds to the formation of the α-PbO_2 and β-PbO_2, respectively. The peak at higher potential (marked as 'c') is assigned as oxygen evolution. The

cathodic peak observed in the potential range of 0.88-0.97 V versus Hg/Hg_2SO_4 electrode (marked as 'd') corresponds to the formation of $PbSO_4$. The inferences of the present study are consistent with the earlier reports [13, 36, 37, 38] in terms of the electrochemical reactions of the ULA and TLA. In order to get a better understanding, the variation in the potential for the formation PbO_2 and $PbSO_4$ during the respective anodic and cathodic half-cycles are plotted as a function of cycles and are shown in the Figs. 8(a to c).
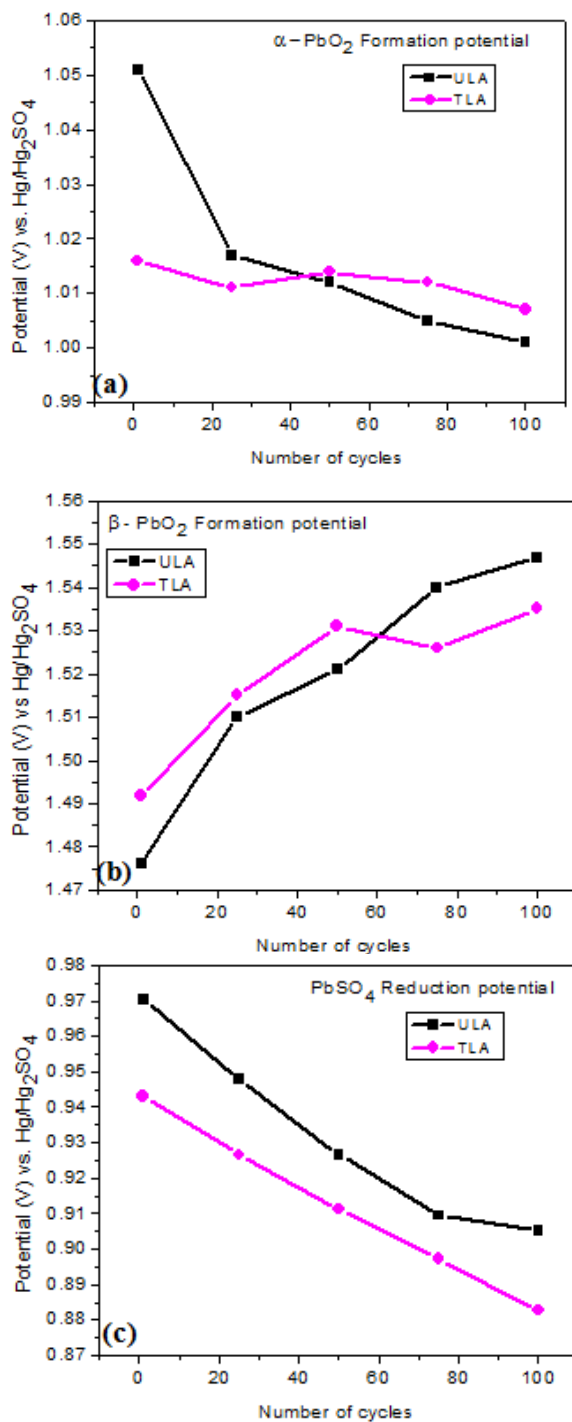

Figure 8. Variation in potential for the formation of PbO_2 and $PbSO_4$ recorded as a function of number of cycles: α-PbO_2 (a); β-PbO_2 (b); and $PbSO_4$ (c).

The extent of change in the potential for the formation of the α-PbO$_2$ and β-PbO$_2$ between the 1st and 100th cycle is relatively less for the TLA when compared to that of the ULA (Figs. 8(a) & (b)), which suggests an improved electrode interface of the TLA. The extent of change in potential for the formation of PbSO$_4$ between the 1st and 100th cycle appears to be similar for both the ULA and TLA (Fig. 8(c)). Both of them exhibit a continuous decrease in potential from 1st to the 75th cycle, which suggests their ability to deliver a better capacity with time. Between the 75th and 100th cycle, saturation in potential is observed for the ULA whereas the TLA exhibits a continuous decrease in potential between these cycles. According to Papazov et al. [39], the PbSO$_4$ crystals formed on smooth surface exhibit a rapid capacity loss. Hence, the continuous decrease in potential from 1st to 100th cycles observed for the TLA could be attributed to an increase its surface roughness and also surface area. In addition, the generation of a more uniform surface profile with dimple-like features and increase in surface roughness of the TLA would help to improve the interfacial characteristics of active material and the alloy grid. The increase in current density in the redox reactions suggests good charge-discharge characteristics of the TLA than that of the ULA.

4. CONCLUSIONS

SMAT induced plastic deformation of Pb-Sn alloy to a depth of ~ 43 µm enabled the formation of a graded layer structure. It increased the average surface roughness (R$_a$) from 0.40 to 2.42 µm. SMAT of the Pb-Sn alloy has resulted in the generation of a uniform surface profile and dimple-like features. No significant change in the grain size and lattice parameter is observed due to the ability of the Pb-Sn alloy to plastically deform and to accommodate the strain induced during SMAT. As a result, only a marginal improvement in hardness is noticed. The formation of an oxide layer offered a better corrosion resistance for the TLA in sulphuric acid medium. The increase in surface roughness and surface area would help to improve interfacial characteristics of the grid and active material. The increased current density for the redox reactions suggests that the TLA would offer good charge-discharge characteristics. The study concludes that SMAT can be used as a pre-treatment process for the Pb-Sn alloy for battery applications.

References

1. D. A. J. Rand, P. T. Moseley, J. Garche and C. D. Parker, *Valve regulated lead acid batteries*, Elsevier, Netherlands, (2004).
2. D. Pavlov, *Lead Acid Batteries: Science and Technology*, Elsevier, Netherlands, (2011).
3. M. D. Achtermann and M. E. Greenlee, *J. Power Sources*, 33 (1991) 87.
4. R. D. Prengaman, *J. Power Sources,* 95 (2001) 224.

5. R. D. Prengaman, in: K. R. Bullock, D. Pavlov, (Eds.), Proceedings Advances in Lead-acid Batteries, *The Electrochemical Society*, Pennington, NJ, 84-14 (1984) 201.
6. W. R. Osório, L. C. Peixoto and A. Garcia, *J. Power Sources*, 194 (2009) 1120.
7. W. R. Osório, C. S. C. Aoki and A. Garcia, *J. Power Sources,* 185 (2008) 1471.
8. E. Rocca and J. Steinmetz, *Electrochim. Acta,* 44 (1999) 4611.
9. R. D. Prengaman, *J. Power Sources,* 158 (2006) 1110.
10. L. Z. Wang, K. Q. Zhang, S. H. Gu and Y. Zhang, *Adv. Mater. Res.,* 335–336 (2011) 826.
11. G. Lin, G. Zhou, D. Li and M. Zheng, *J. Rare Earths,* 24 (2006) 232.
12. A. J. Li, H. Y. Chen and R. Z. Li, *Adv. Mater. Res.,* 156–157 (2011) 1046.
13. Y. B. Zhou, C. X. Yang, W. F. Zhou and H. T. Liu, *J. Alloys Compds,* 365 (2004) 108.
14. W. X. Guo, D. Shu, H. Y. Chen, A. J. Li , H. Wang, G. M. Xiao, C. L. Dou, S. G. Peng, W. W. Wei, W. Zhang, H. W. Zhou and S. Chen, *J. Alloys Compds,* 475 (2009) 102.
15. W. R. Osório, C. S. C. Aoki and A. Garcia, *Mater. Sci. Forum,* 595–598 (2008) 851.
16. W. R. Osório, P. R. Goulart, G. A. Santos, C. Moura Neto and A. Garcia, *Metall. Mater. Trans, A* 37 (2006) 2525.
17. W. R. Osório, D. M. Rosa and A. Garcia, *J. Power Sources,* 175 (2008) 595.
18. D. M. Rosa, J. E. Spinelli, W. R. Osório and A. Garcia, *J. Power Sources,* 162 (2006) 696.
19. L. C. Peixoto and W. R. Osório, *J. Power Sources,* 192 (2009) 724.
20. S. Rashkov, Y. Stefanov, Z. Noncheva, M. Petrova, T. Dobrev, N. Kunchev, D. Petrov, S. Vlaev, V. Mihnev, S. Zarev, L. Georgieva and D. Buttinelli, *Hydrometallurgy,* 40 (3) (1996) 319.
21. R. David Prengaman and A. Siegmund, copper 99-cobre-99 International symposium (phoenix Arizona), 10-13 (1999) 1.
22. V. F. Bashev, N. E. Zhitnik, V. A. Ivanov, D. A. Rybalka, Tkachenko and A. Yu, *Russ. Metallurgy (Metally),* 1 (2011) 85.
23. D. A. J. Rand, D. P. Boden, C. S. Lakshmi, R. F. Nelson and R. D. Prengaman, *J. Power Sources,* 107 (2002) 280.
24. J. C. Caicedo, L. Yate, G. Cabrera, W. Aperador, G. Zambrano and P. Prieto, *J. Mater. Sci.,* 46 (2011) 1244.
25. T. Y. Lin and C. T. Lee, *J. Alloys Compds,* 542: (2012) 11.
26. L. F. Hou, Y. H. Wei, X. F. Shu and B. S. Xu, *J. Alloys Compds,* 492 (2010)   347.
27. M. Laleh and F. Kargar, *J. Alloys Compds,* 509 (2011) 9150.
28. K. Lu and J, Lu, *J.Mater. Sci. Technol.,* 15 (1999) 193.
29. K. Lu and J. Lu, *Mater. Sci. Eng. A*, 375–377 (2004) 38.
30. T. Balusamy, Satendra Kumar and T. S. N. Sankara Narayanan, *Corros. Sci.,* 52 (2010) 3826.
31. D. Li, H. N. Chen and H. Xu, *Appl. Surf. Sci.,* 255 (2009) 3811.
32. B. Arifviantoa, Suyitnoa, M. Mahardika, P. Dewoa, P. T. Iswantoa and U. A. Salima, *J. Mater. Chem. Phys.,* 125 (2011) 418.
33. S. Anand Kumar, S. Ganesh Sundara Raman, T. S. N. Sankara Narayanan and R. Gnanamoorthy, *Surf. Coat. Technol.,* 206 (2012) 4425.
34. G. Singh Mann and G. Blanc, MI (US) Patent No. 6,833,218 B2 Dec.21 2004.
35. M. Laleh and F. Kargar, *J. Alloys Compds*, 509 (2011) 9150.
36. G. Baril, C. Blanc and N. Pebere, *J. Electrochem. Soc.,* 148 (2001) B489.
37. B. Monahov, D. Pavlov, A. Kirchev and S. Vasilev, *J. Power Sources,* 113 (2003) 281.
38. D. Pavlov, A. Kirchev, M. Stoycheva and B. Monahov, *J. Power Sources,* 137 (2004) 288.
39. G. Papazov, D. Pavlov and B. Monahov, Proc. Vol.II, *4ᵗʰ ALABC members & Contractors conference*, Scottsdale, AZ, USA, April (1999) 425.